Figure 1(a).   Broadband *Chandra* image of Tycho's SNR. The southernmost portion is not imaged.

the highest spatial resolution that has been obtained to date in X-rays. The third panel of Fig. 3 shows an "equivalent width" image of the Si He α blend near 1.86 keV, where the underlying continuum has been subtracted at each point in the Si image, and the ratio formed between the remaining line emission and the continuum. Such an image indicates where the Si element abundance (tracked by the relative strength of the Si line emission) is high. Most of the Si line emission is associated with ejecta because they require element abundances that are enhanced well above the solar values. This implies that the Si ejecta are distributed throughout the remnant, including at many positions near the edge of the remnant at the position of the forward shock.

2. Spectral observations

With *Chandra*'s superb spatial resolution, moderate resolution X-ray spectra can be obtained for any region of the remnant for which there are sufficient numbers of photons. Some spatially resolved spectra of compact regions obtained by *XMM-Newton* were presented by Decourchelle *et al.* (2001). Here we present a small sample of spectra on even smaller spatial scales from *Chandra*.

2.1 *Forward shock*

Chandra is able to obtain the spectrum of the thin rim and provide the first X-ray spectrum of the forward shock in this young, historical remnant. The spectrum shown on the left of Fig. 2 was taken from a portion of the northwest rim that is bright in
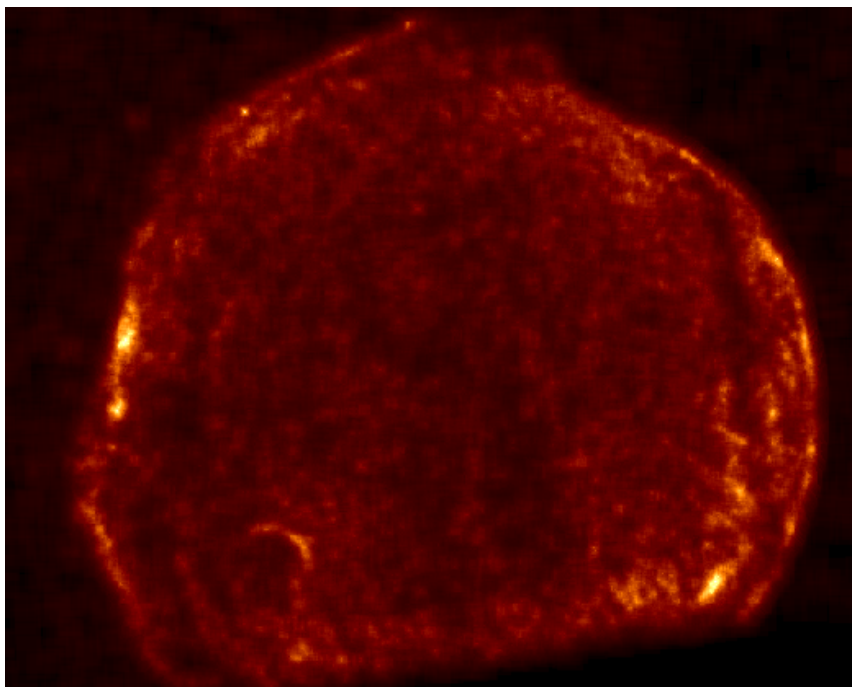
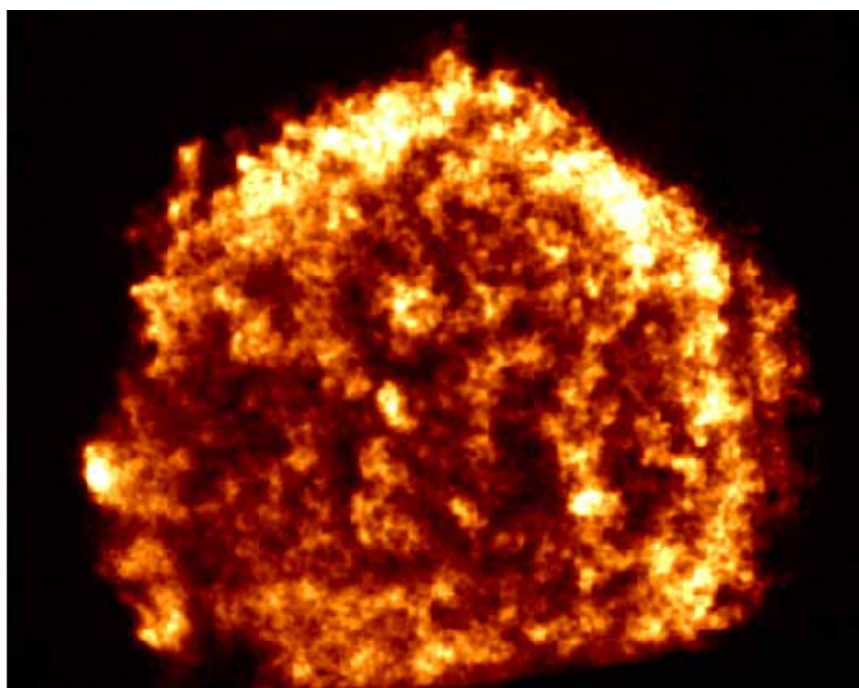**Figure 1(b).** Image in the X-ray continuum at energies between 4 and 6 keV.

Figure 1(c). Equivalent width image (line to continuum ratio) of the Si He α blend near 1.86 keV.
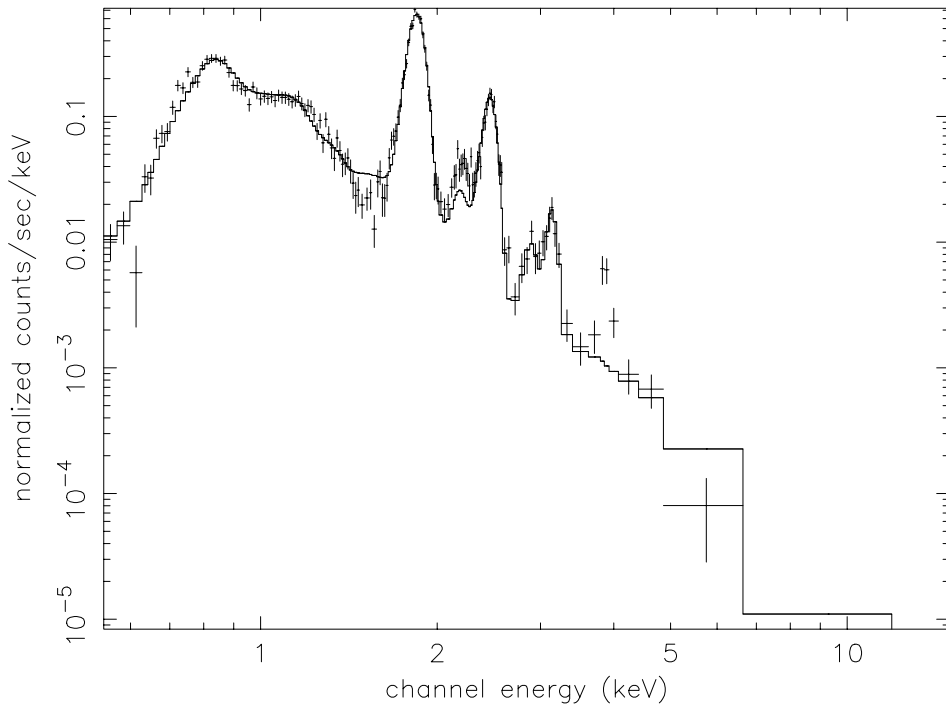
Tycho's SNR Si—rich Knot

Figure 3(a). Spectrum of the Si-rich knot in the east.

the 4–6 keV continuum. It is nearly devoid of line features, and can be described either by a nonthermal synchrotron spectrum (we used one with an exponential cutoff in the electron distribution function, taking the cutoff frequency from Reynolds & Keohane (1999), and radio spectral indices from Katz-Stone *et al.* 2000), or by a thermal spectrum with very low ionization parameters and a temperature near 2 keV, or by a combination of these.

It is unfortunately not possible to distinguish between thermal and nonthermal scenarios on the basis of the *Chandra* spectra alone. Energy coverage is needed above 10 keV, where the curvatures in the spectra predicted by these models diverge more strongly. Nevertheless, it seems likely that some of the X-ray emission is nonthermal, as there is overall an excellent correspondence between the X-ray and radio outlines at the forward shock (Dickel *et al.* 1991). The nonthermal X-ray emission could come from a population of electrons accelerated to high energies at the shock in the same way as the electrons responsible for the radio emission. Moreover, the radio images show that this northwest arc is also bright in radio emission. Given that there is hard emission detected from the remnant as a whole at energies up to 25–30 keV, it is plausible that a nonthermal emission component coming from the forward shock could be associated with this hard emission.

If this emission is predominately thermal, it shows low electron temperatures compared to the roughly 4600 km/s expansion velocities measured for Tycho's SNR in X-rays (Hughes 2000). The spectra of other regions around the rim are qualitatively

to the background subtraction), but the dominant spectral features are due to the Fe L emission. The spectra are fitted with nonequilibrium ionization thermal models.

3. Summary

Chandra and *XMM-Newton* have inaugurated the era of true spatially resolved X-ray spectroscopy. For supernova remnants like Tycho's SNR, this means the capability to measure, for the first time, the detailed distribution of the ejecta and the spectra of ejecta at different positions in the remnant. It also reveals the spectra at the forward shock, which most likely arise from both nonthermal and thermal emission processes.

References

Decourchelle, A., *et al.* 2001, *A&A*, **365,** L218.

Dickel, J. R., *et al.* 1991, *A. J.*, **101,** 2151.

Hughes, J. P. 2000, *Ap. J.*, **545,** L53.

Hwang, U., Gotthelf, E. V. 1997, *Ap. J.*, **475,** 665.

Katz-Stone, D. M., *et al.* 2000, *Ap. J.*, **529,** 453.

Reynolds, S. P., Keohane, J. W. 1999, *Ap. J.*, **525,** 368.

Seward, F., *et al.* 1983, *Ap. J.*, **266,** 287.

Vancura, O., Gorenstein, P., Hughes, J. P. 1995, *Ap. J.*, **441,** 680.

Table 1. General information on the program stars. Δm is difference in magnitude between the maximum and minimum of light curve in a filter and σ is the standard deviation of the difference in magnitude of comparison stars.

X-ray source	Optical counterpart	V (mag)	Co-ordinate (2000)	Filter	Δm (mag)	σ (mag)	$\Delta m/\sigma$
1ES 0829+15.9	MCC 527	10.41	$\alpha = 08^h 32^m 30^s$	B	0.111	0.007	14.1
			$\delta = 15^0 49' 26''$	V	0.114	0.006	17.9
				R	0.103	0.007	14.7
1ES 0920-13.6	HD 81032	9.02	$\alpha = 09^h 22^m 53^s$	B	0.300	0.025	12
			$\delta = -13^0 49' 43''$	V	0.284	0.014	19.7
				R	0.261	0.014	18.4
WFC J1102.0+2235	HD 95559	8.96	$\alpha = 11^h 02^m 02^s$	B	0.080	0.012	6.7
			$\delta = 22^0 35' 45''$	V	0.076	0.012	6.3
				R	0.060	0.009	6.7
1ES 1737+61.2	HD 160934	10.29	$\alpha = 17^h 38^m 30^s$	B	0.116	0.012	9.7
			$\delta = 61^0 15' 09''$	V	0.111	0.014	8.0
				R	0.080	0.009	8.9

mode of 2×2 pixel^2, where each super pixel corresponds to 0.72×0.72 arcsec^2. The CCD covers a field of view $\sim 13 \times 13$ arcminute^2.

Multiple CCD frames were taken with the exposure time ranging from 2 to 120 secs depending on the seeing conditions and the filters used. A number of bias and twilight flat field frames were also taken during the observing run. The frames were cleaned employing the IRAF/MIDAS software. The differential magnitude of the stars were determined by aperture photometry.

3. Analysis and light curve

Three comparison stars for each program star (2 for HD 95559), having magnitude and colour similar to the program star and in the same CCD frame, were used to check for the variability in the program stars. Pair wise differential magnitudes of the comparison stars were computed and the standard deviations (σ) examined. In each case, the standard deviations were found to be nearly equal. Further analysis was carried out with only one of the comparison stars, closest to the program star. The ratio $\Delta m/\sigma$ indicates that all the program stars show statistically significant variability. In each filter, Δm, the difference between the maxima and the minima of the light curves was also determined. The light curves were analysed for periodicity using the Lomb-Scragle periodogram method in Starlink's Period software, and by fitting a sinusoidal function using the least square deviation method. Results from this analysis for each variable star are given below.

3.1 *1ES 0829+15.9 (MCC 527)*

Light curves obtained for MCC 527 in the B,V and R filters are shown in Fig. 1 (left panel). MCC 527 is a K8 spectral type star (A. V. Kazarovets *et al.* 1999), and is also listed as an unsolved variable (FR Cnc) in the Hipparcos catalogue (Perryman *et al.* 1997). Measurements with the Hipparcos satellite (Perryman *et al.* 1997) provide